HHS Public Access

Author manuscript

Biol Psychiatry. Author manuscript; available in PMC 2021 April 01.

Published in final edited form as:

Biol Psychiatry. 2020 April 01; 87(7): 619–631. doi:10.1016/j.biopsych.2019.07.024.

Altered corticolimbic control of the nucleus accumbens by chronic Δ⁹-THC

Eun-Kyung Hwang, **Carl R. Lupica**

Electrophysiology Research Section, Intramural Research Program, National Institute on Drug Abuse, National Institutes of Health, Baltimore, Maryland 21224

Abstract

Background: Decriminalization, legalization and expansion of medical cannabis has led to an increase in its use and availability of high-potency strains. Cannabis potency is determined by the concentration of Δ^9-tetrahydrocannabinol (Δ^9-THC), a psychoactive constituent that activates CB1 and CB2 cannabinoid receptors (CB1R, CB2R), and use of high-potency cannabis is associated with cannabis use disorder (CUD) and increased susceptibility to psychiatric illness. The nucleus accumbens (NAc) is part of a brain reward circuit affected by Δ^9-THC through modulation of glutamate afferents arising from corticolimbic brain areas implicated in drug addiction and psychiatric disorders. Moreover, brain imaging studies show alterations in corticolimbic and NAc properties in human cannabis users.

Methods: Using *in vitro* electrophysiology and optogenetics, we examine how Δ^9-THC alters corticolimbic input to the NAc in rats.

Results: We find that chronic Δ^9-THC weakens prefrontal cortex glutamate input to the NAc shell (NAcs) and strengthens input from basolateral amygdala and ventral hippocampus. Further, whereas chronic Δ^9-THC had no effect on net strength of glutamatergic nput to NAcs arising from midbrain DA neurons, it alters fundamental properties of these synapses.

Conclusions: Chronic Δ^9-THC shifts control of the NAcs from cortical to limbic input likely contributing to cognitive and psychiatric dysfunction associated with cannabis use.

Keywords

cannabis; cannabinoid; glutamate; long-term depression; marijuana; medicinal marijuana; synapse

Corresponding author: Carl Lupica, Ph.D., Chief, Electrophysiology Research Section, 251 Bayview Blvd, NIDA-IRP, NIH, Baltimore, Maryland 21224, Tel: (443) 740-2824, clupica@mail.nih.gov.

Disclosures

The authors report no biomedical financial interests or potential conflicts of interest.

Introduction

Extensive data show that synaptic changes in neural circuits involved in learning and motivation are associated with behavioral correlates of drug addiction (1, 2). The nucleus accumbens (NAc) is a focus of these studies because of its central role in motivation and reward, and because it shows progressive changes in animal addiction models and in human drug users (3–5). These studies indicate that cellular and synaptic mechanisms that exist to support NAc plasticity are coopted by abused drugs to confer persistent synaptic changes underlying compulsive behaviors and addiction (6–8). Thus, withdrawal from psychostimulants like cocaine can increase NAc medium spiny neuron (MSN) sensitivity to glutamate (4, 9), leading to development of addictive behavior (10–12). However, in comparison to extensive data with psychostimulants, the extent to which other drugs alter glutamate signaling is not well understood.

Cannabis is a psychoactive drug used by an estimated 183 million users worldwide (13), and its use is increasing in North America because of decriminalization, legalization, and expansion of medicinal and recreational availability (13). Although often perceived to have few adverse effects, there is increasing evidence for serious psychiatric effects of cannabis (14, 15), and an increased potential for chronic abuse (16, 17), that are likely related to high concentrations of Δ^9-THC found in modern strains (18, 19). Clinically significant symptoms can lead to the diagnosis of Cannabis Use Disorder (CUD), as recognized in the DSM-5 (20, 21). Moreover, brain imaging in individuals with a CUD diagnosis shows changes in regions overlapping those in subjects dependent upon other abused drugs (22), and blunted reactivity of the NAc to psychostimulant challenge (23).

The primary psychoactive constituent of cannabis, Δ^9-THC, activates G-protein-coupled cannabinoid CB1Rs, and CB2Rs (24–26), and this can increase DA release in the NAc (27, 28); a property shared with other abused drugs (29). The axons of ventral tegmental area (VTA) DA neurons project to NAc, and many of these co-release glutamate (30, 31), although the consequences of this are not understood (32, 33). The NAc receives other glutamate inputs from a corticolimbic network including the medial prefrontal cortex (mPFC), ventral hippocampus (vHipp), and basolateral amygdala (BLA). These inputs are integrated by NAc MSNs, and dysfunction within these pathways contributes to drug addiction and other psychiatric disorders (34–36), and brain imaging studies in chronic cannabis users show that inputs to the NAc are altered in association with heightened anxiety and dysregulated cognition (20, 23, 37–41).

Previous studies indicate that Δ^9-THC exposure leads to altered NAc excitatory synaptic transmission and synaptic plasticity (42, 43), but the source of these afferents was not identified, and changes in distinct NAc pathways remain unknown. Here, we examined patterns of altered function in several glutamatergic inputs to the NAc after chronic Δ^9-THC in rats. We find that chronic Δ^9-THC shifts the strength of glutamatergic activation of NAc from cortical to sub-cortical limbic sites, and we hypothesize that this contributes to deleterious effects of cannabis in humans.

Methods and materials

Animals

Wildtype and TH*cre* male Long-Evans rats were 6 to 8 weeks old when surgery was performed and 14–17 weeks old at the time of electrophysiolog1ical recordings. Experimental procedures were approved by the Animal Care and Use Committee of the NIDA Intramural Program.

Virus injection

Intracranial injections of ChR2-expressing viral vectors were performed using published techniques and are described in detail in Supplementary Methods.

Δ^9-THC injection

Δ^9-THC (NIDA Drug Supply), suspended in Tween-80, DMSO and saline (1:2:7) was injected intraperitoneally (i.p.) at 5 mg/kg/day for 14d. Other groups received either vehicle injections, the CB1R antagonist AM251 (2mg/kg, i.p.; Tocris) alone, or AM251, 30 min before each Δ^9-THC injection for 14d.

Electrophysiology

Brain slice preparation and general recording methods were as previously described and are presented in detail in Supplementary Methods.

Optically elicited EPSCs (oEPSCs) were evoked at 0.033 Hz using 473-nm laser pulses (2 ms duration) collimated through the objective. Picrotoxin (100 μM) blocked $GABA_A$ receptors. Input-output (I-O) relationships between oEPSC amplitude and laser intensity (0.2, 0.7, 1.1, 2.0, 3.3, 5.1, 7.1 mW, measured at the objective) were constructed. To maintain consistency across slices and brain areas, we used the same injection volume of ChR2 virus (0.7 μl), the same duration to permit transfection (6–8 weeks), and the same oEPSC threshold criterion (1–3 mW). Ratios of pairs of oEPSCs (paired-pulse ratio; PPR) were collected using two laser stimuli with 20, 50, 75, 100, or 250 ms inter-stimulus intervals (ISI). The ratio was calculated by averaging 5 consecutive responses and dividing the peak amplitude of the second oEPSC by the first.

AMPAR/NMDAR ratios were calculated by measuring oEPSCs (having AMPAR and NMDAR components) at +40 mV, followed by recordings at −70 mV during NMDAR antagonist (DL-2-Amino-5-phosphonopentanoic acid; DL-AP5; 100 μM) application. NMDAR-mediated currents were calculated by subtracting oEPSCs recorded in DL-AP5 from currents measured at +40 mV [AMPAR/NMDAR ratio = peak AMPAR oEPSC at −70 mV/EPSC at +40 mV].

The rectification index (RI) was calculated using oEPSCs averaged at −70mV, 0mV, and +40mV (corrected for a 10 mV junction potential) and normalized to the oEPSC at −70mV. RI was calculated as the ratio of slope of current-voltage (I-V) relationship at −70 mV and +40 mV (RI = [EPSC-70mV/(−70-Erev)]/[EPSC+40mV/(+40-Erev)]). Sensitivity of oEPSCs to NASPM (N-[3-[[4-[(3-aminopropyl)amino]butyl]amino]propyl]-1-

naphthaleneacetamide; 50 μM) was determined after a 10 min baseline at −70 mV. Spermine (0.1 mM) was included in the pipette solution for RI and NASPM experiments. Laser-evoked NMDAR currents (oNMDA) were −80mV to +40 mV. During AMPAR (6,7-Dinitroquinoxaline-2,3-dione; DNQX) and $GABA_A$ receptor (picrotoxin) block. Onmda I-V relationships were measured at holding potentials from −80mV to +40 mV.

Drugs

DL-AP5, DNQX, NASPM, (*S*)-3,5-Dihydroxyphenylglycine (DHPG), and AM251 were purchased from Tocris (Bristol, United Kingdom), and picrotoxin from Sigma-Aldrich (St Louis, MO, USA). Drug application and data analysis are described in detail in Supplementary Methods

Results

Chronic Δ^9-THC increased MSN action potential threshold to a small degree, suggesting some direct effects of Δ^9-THC on neuronal excitability (Fig. S2).

Altered NAcs synaptic transmission following Δ^9-THC treatment

Following ChR2 expression using a CAMKII promoter in wildtype rats (mPFC, vHipp, BLA), or a *cre*-driven promoter in TH*cre* transgenic rats (VTA) (Fig. 1A), dense eYFP fluorescence was observed in NAcs and at the sites of injection (Fig. 1A, Fig. S1). To facilitate comparisons among inputs to the NAcs we examined the largest oEPSCs that could be evoked by laser activation of ChR2. In vehicle-injected controls, the maximum oEPSCs generated by stimulating mPFC, vHipp and BLA NAcs afferents were similar in size (Fig. 1). However, those generated by VTA inputs were significantly smaller (Fig. 1A, 1B).

24 hours after the final Δ^9-THC injection, maximum oEPSCs from vHipp and BLA inputs were significantly increased (Fig. 1), whereas mPFC-activated oEPSCs were significantly smaller compared to control (Fig. 1B). Maximum oEPSCs originating from VTA afferents to NAcs were unchanged following Δ^9-THC injections (Fig. 1B, 1F). The changes in maximum oEPSCs caused by Δ^9-THC in the mPFC, vHipp, and BLA were prevented by AM251 given before each Δ^9-THC injection (Fig. 1C–E), whereas AM251 alone had no effect at any of the NAcs afferents (Fig. 1C–F). Thus, chronic Δ^9-THC differentially altered the strength of excitatory input to the NAcs, such that cortical (mPFC) input was weakened (Fig. 1B–C), and limbic (vHipp and BLA) input was strengthened (Fig. 1B, Fig. 1D–E) via actions at CB1Rs (Fig. 1C–E).

Mechanisms of weakened synaptic transmission at mPFC to NAc synapses following chronic Δ^9-THC.

We next examined the mechanisms through which chronic Δ^9-THC reduced maximal mPFC-generated oEPSC in NAcs (Fig. 1). The I-O curve plotting oEPSCs across a range of laser intensities was significantly decreased following chronic Δ^9-THC (Fig. 2A). Glutamate release probability was then measured using oEPSCs evoked by paired-laser stimuli at varying ISIs. In chronic-vehicle cells oEPSC2 was smaller than oEPSC1 at all ISIs, yielding a paired-pulse ratio (PPR) ≤ 1.0 (Fig. 2B), which is consistent with the reported high

probability of glutamate release at Mpfc → NAcs synapses (45, 46). However, the PPR was significantly increased in cells from Δ^9-THC-treated rats (Fig. 2B), suggesting a decrease in glutamate release probability. To corroborate this, we measured use-dependent blockade of oNMDA currents at +40mV (at 15 s intervals) using the NMDA open-channel blocker MK801 (47, 48). Since the rate of block by MK801 depends on the proportion of NMDA channels opened by glutamate, oNMDA currents are more quickly inhibited when release probability is high. Compared to MSNs recorded in chronic vehicle, or Δ^9-THC + AM251 animals, oNMDA inhibition by MK801 in the Δ^9-THC group required significantly more laser stimuli to achieve the same degree of inhibition (Fig. 2C), consistent with lower glutamate release probability. oNMDA I-V curves showed that the voltage-dependency of NMDA channels was unaffected by chronic Δ^9-THC at mPFC → NAcs synapses (Fig. 2D). These data suggest that glutamate release probability was reduced by chronic Δ^9-THC, and this contributed to weakened mPFC input to NAcs.

The inward rectification of EPSCs at depolarized membrane potentials is observed when tetrameric AMPA receptors lack the GluR2 (GluA2) subunit (49, 50). AMPARs lacking GluR2 also 8 generate larger EPSCs and have higher permeability to Ca^{2+} (49), leading to their designation as Ca^{2+}-permeable (CP-AMPAR), or Ca^{2+}-impermeable (CI-AMPAR) AMPA receptors (50–52). The proportions of CP- and CI-AMPARs at central synapses is influenced by environmental factors and drugs that affect GluR2 incorporation, and/or AMPAR number (8, 51, 53, 54). We measured inward rectification of oEPSCs at mPFC → NAcs synapses using the rectification index (RI, Fig. 2E) and found that it was significantly smaller in neurons from chronic Δ^9-THC animals, and this was prevented by pre-treatment with AM251 (Fig. 2E, 2F). Thus, chronic Δ^9-THC caused a proportional shift from GluR2-lacking AMPARs to GluR2-containing AMPARs, and this contributed to weakening these synapses. These results suggest that chronic Δ^9-THC reduced the strength of mPFC → NAcs glutamate synapses via pre-and postsynaptic mechanisms.

Mechanisms of strengthened vHipp glutamatergic input to NAc following chronic Δ^9-THC

As predicted from larger maximum oEPSCs (Fig. 1), the I-O relationship for the vHipp → NAcs pathway was significantly increased by chronic Δ^9-THC (Fig. 3A), and this was prevented by AM251 (Fig. 1D). To determine mechanisms of this change we measured glutamate release probability using PPR and found that it was altered only at the 75 ms ISI (Fig. 3B). Also, the activity-dependent block of oNMDA currents by MK801 was unchanged by chronic Δ^9-THC (Fig. 3C), suggesting a small effect of chronic Δ^9-THC on glutamate release at these synapses.

To investigate whether postsynaptic properties were altered by Δ^9-THC, we measured the ratio of AMPA receptor oEPSCs to oNMDA currents. The AMPA/NMDA ratio increased significantly after chronic Δ^9-THC (Fig. 3D), but this was not prevented by AM251 (Fig. 3D), suggesting that the effect was not mediated by CB1Rs. Since AMPA/NMDA ratios can reflect changes in either current, we constructed oNMDA I-O curves and found a significant reduction at only the highest laser intensity (7.1 mW, Fig. 3E), and an unchanged I-V curve (Fig. 3F). To determine whether NMDAR subunits were altered, we examined oNMDA inhibition by the NR2B-subunit (GluN2B) antagonist, ifenprodil. Ifenprodil inhibited

oNMDA currents similarly in neurons from all groups (Fig. S3), suggesting that although NR2B subunits exist at vHipp → NAcs synapses, their contribution to oNMDA currents not affected by chronic Δ^9-THC. The data indicate that a small decrease in oNMDA currents at vHipp → NAcs synapses after chronic Δ^9-THC, but this is unlikely to contribute to the strengthening of this projection.

We next determined the effects of chronic Δ^9-THC on AMPARs and found a significant increase in the RI (Fig. 3G). Consistent with this, oEPSCs from neurons in the Δ^9-THC group were significantly inhibited by the inhibitor of CP-AMPARs, NASPM (55; Fig. 3H). The data suggest that the increase in CP-AMPRs likely contributed to strengthening of the vHipp → NAcs input by chronic Δ^9-THC.

Mechanisms of strengthened BLA glutamatergic input to NAc following chronic Δ^9-THC.

Consistent with the increase in maximal EPSCs at the BLA → NAcs projection (Fig. 1), the I-O relationship was significantly increased by chronic Δ^9-THC, and this was prevented by AM251 (Fig. 4A). However, although PPRs were unchanged (Fig. 4B), suggesting that glutamate release probability was unaltered, the rate of blockade of oNMDA currents by MK801 was faster in neurons from the Δ^9-THC treatment group, suggesting an increase in release probability (Fig. 4C). To reconcile these contradictory findings, we measured oNMDA properties, and found a significantly smaller I-O relationship (Fig. 4E), and an unchanged oNMDA I-V curve following chronic Δ^9-THC (Fig. 4F). This suggests that the number of synaptic NMDARs was reduced, but their voltage-dependence was unchanged by Δ^9-THC. Therefore, the increased rate of MK801 blockade of oNMDA currents (Fig. 4C) may have resulted from fewer synaptic NMDARs, rather than altered glutamate release probability. Consistent with this, the BLA → NAcs AMPA/NMDA ratio was significantly increased following chronic Δ^9-THC. However, this was not prevented by pre-treatment with AM251 (Fig. 4D), perhaps indicating a lack of CB1R involvement.

We next analyzed the RI of AMPA-oEPSCs at BLA → NAcs synapses and found no significant effect of chronic Δ^9-THC (Fig. 4G). Consistent with the absence of Δ^9-THC effects on AMPAR subunits, the effect of NASPM on oEPSCs was similar in neurons from vehicle and Δ^9-THC treated groups (Fig. 4H). Therefore, in the absence of changes in AMPAR subunits and a decrease in NMDAR number, the data suggest that the strengthened BLA → NAcs I-O relationship likely occurred via an increase in the number of synaptic AMPARs following chronic Δ^9-THC.

Homeostatic plasticity at VTA to NAcs synapses following chronic Δ^9-THC exposure

Many midbrain DA neurons co-express tyrosine hydroxylase (TH), and the vesicular glutamate transporter-2 protein (vGluT2) (30, 31), and co-release DA and glutamate in NAc (32, 33). We examined effects of chronic Δ^9-THC on NAcs glutamate release from these VTA neurons using ChR2 expression in THCre rats. Congruent with the lack of Δ^9-THC effects on maximum oEPSCs in the VTA → NAcs pathway (Fig. 1B, 1C), the I-O curve was also unchanged (Fig. 5A). However, despite this apparent absence of effects, PPR curves were significantly reduced in an AM251-sensitive manner by chronic Δ^9-THC at these synapses (Fig. 5B), suggesting an increase in glutamate release probability.

We next found that the RI for VTA → NAcs AMPA oEPSCs was significantly increased by chronic Δ^9-THC (Fig. 5C), and this was prevented by AM251 (Fig. 5C), suggesting a shift from CI-AMPARs to CP-AMPARs. This was confirmed by the significant inhibition of oEPSCs by NASPM in cells only from the chronic Δ^9-THC group (Fig. 5D), which was prevented by AM251 co-treatment (Fig. 5D). In contrast to these RI data, AMPA/NMDA ratios showed no differences among groups. Together, these data suggest that although net synaptic strength was unaltered by Δ^9-THC at VTA → NAcs glutamate synapses, there was an increase in both glutamate release probability and the proportion of GluR2-lacking CP-AMPARs.

Synapse-specific effects of chronic Δ^9-THC on group-I metabotropic glutamate receptor-mediated long-term depression.

When activated by glutamate or agonists like DHPG, group-I metabotropic glutamate receptors (mGluRIs) can initiate long-term depression (LTD) of glutamatergic synaptic transmission in the NAcs, and this is impaired by Δ^9-THC (34, 42, 43, 56). However, few studies have investigated mGluRI-LTD of distinct glutamate NAcs afferents (57–59), and effects of Δ^9-THC on LTD at individual NAc afferents by is unknown. Therefore, we examined the effects of chronic Δ^9-THC on mGluRI-LTD at mPFC, vHipp, BLA, and VTA NAcs inputs. DHPG (50 μM, 10 min) caused LTD at mPFC, vHipp, and BLA NAcs afferents following chronic vehicle (Fig. 6A–C), but LTD was not observed at VTA inputs (Fig. 6D). Following chronic Δ^9-THC, DHPG-LTD was significantly impaired at mPFC and vHipp NAcs inputs (Fig. 6A, 6B), and this was prevented by AM251 (Fig. 6Ea, 6Eb). However, DHPG-LTD was not affected by chronic Δ^9-THC at BLA inputs to the NAcs.

Discussion

Our study shows that chronic Δ^9-THC disrupts the balance of corticolimbic glutamate input to the NAcs, weakening PFC inputs, and strengthening those from BLA and vHipp. Moreover, mGluRI-LTD was also absent in the mPFC and vHipp pathways to NAcs following Δ^9-THC. These results suggest that Δ^9-THC alters the interaction among neuronal pathways involved in regulating NAcs output, likely changing its control over motivation, cognition and emotion. Most of the effects of chronic Δ^9-THC were prevented by the CB1R antagonist AM251, suggesting this is the primary molecular site where the phytocannabinoid acts. However, some Δ^9-THC effects were not prevented by AM251, suggesting CB2R involvement, heterogeneous responses by D1 receptor (D1R)- and D2R-expressing MSNs, or other off-site effects (60). Importantly, the dose of Δ^9-THC used in our experiments (5 mg/kg) results in blood concentrations in rodents (50–150 ng/mL) (61) similar to those measured in human marijuana smokers (62). Also, as we previously reported that Δ^9-THC is not detectable using LC-MS in rodent brain 1 day after the last of 7 daily injections (10 mg/kg) (63), it is likely that the amount of brain exposure to Δ^9-THC in our study approximates that in human marijuana users, and that the present results were unaffected by residual brain levels of the phytocannabinoid.

The weakening of mPFC input to NAcs following chronic Δ^9-THC involved pre-and postsynaptic mechanisms, including decreased glutamate release probability and an

increased proportion of low-conductance, GluR2 subunit-containing, CI-AMPARs. In contrast, the strengthening of vHipp glutamatergic input to NAcs occurred postsynaptically, similar to long-term potentiation described at other synapses (8, 64, 65). Thus, vHipp → NAcs synapses showed no change in glutamate release probability, an increase in high-conductance CP-AMPARs, and an increased AMPA/NMDA ratio, which is indicative of increased AMPAR number or single channel current (7, 66, 67). Similar patterns of AMPAR changes at NAc afferents (12, 51, 57, 59, 68), and at vHipp → NAcs synapses (69) have been described after cocaine exposure. Interestingly, vHipp activation increases VTA DA neuron firing and NAc DA release (70, 71), and cannabinoid-induced enhancement of vHipp activity is linked to schizophrenia-like behavior in rats (72). Thus, vHipp inputs to NAcs are vulnerable to strengthening by distinct classes of abused drugs resulting in enhancement of NAcs DA release to perhaps increase susceptibility to psychiatric disorders and addiction.

In contrast to mPFC and vHipp inputs, alterations in VTA and BLA NAcs afferents by Δ^9-THC were more complex. Thus, BLA → NAcs input was strengthened and AMPA/NMDA ratio increased by chronic Δ^9-THC, indicating synaptic potentiation. Although PPRs indicated that glutamate release probability was unchanged at BLA inputs, MK801 inhibited oNMDA currents faster following chronic Δ^9-THC, suggesting increased release probability (47, 48). However, the oNMDA I-O relationship was reduced without a change in voltage-sensitivity, suggesting that NMDA receptor numbers decreased at BLA → NAcs synapses following chronic Δ^9-THC. Since the rate of blockade of oNMDA currents by MK801 depends on the proportion of channels activated by each stimulus (47), the faster block after Δ^9-THC likely resulted from fewer NMDA receptors, rather than altered glutamate release. As neither the RI, nor sensitivity to NASPM were changed by chronic Δ^9-THC at BLA → NAcs synapses, the pattern of results suggest that this pathway was strengthened via an increase in AMPARs with no change in subunit composition (9). Moreover, as NMDARs did not contribute to oEPSCs at −70 mV (Fig. 4F), the decrease in NMDARs likely did not contribute to increased synaptic at BLA → NAcs synapses, although this diminished NMDAR influence could reduce their contribution to other cellular processes such as plasticity. The large increase in BLA → NAcs strength caused by chronic Δ^9-THC may enhance its reported involvement in processing contextual drug-associated cue information (73).

The discovery of VTA neurons expressing both TH and VGluT2 suggest DA-glutamate co-transmission to the NAc (31–33, 74, 75), but the consequences of this remain poorly-understood (76). We expressed ChR2 in VTA TH*cre* neurons to study the glutamate input to the NAcs and found that it was much weaker than the other pathways we examined. Moreover, whereas chronic Δ^9-THC had no effect on the net strength of this input, both glutamate release probability and the proportion of CP-AMPARs was increased. We speculate that a homeostatic rebalancing of AMPAR number occurred to offset increases in release and CP-AMPARs (77). However, these changes may have other consequences since CP-AMPARs enhance dendritic calcium and this could alter local signaling mechanisms.

Distinct glutamate pathways to the NAc can target the same populations of MSNs, and mediate different behavioral and physiological responses (78–83). This suggests that individual MSNs integrate overlapping inputs, and that alterations in this balance can bias

downstream information flow. The impact of this integration has been demonstrated by activating these inputs singularly or in combination. Thus, activation of PFC input to NAc alone does not drive MSN spike activity, but when combined with vHipp activation action potentials are observed (79). The weakened PFC input to NAc that we observe after Δ^9-THC would strongly restrict PFC contributions to synaptic integration at MSNs, whereas the strengthened BLA and vHipp inputs would greatly increase their influence on NAc output. Given the demonstrated importance of these pathways in addiction and psychiatric disorders, these Δ^9-THC-mediated changes could contribute to cognitive, emotional and behavioral issues observed in chronic cannabis users.

The involvement of mGluRIs in LTD of NAc glutamatergic neurotransmission has been described using electrical stimulation and selective activation of NAc afferents (43, 53, 56, 57). These studies show that mGluRI-LTD requires retrograde endocannabinoid activation of CB1Rs and altered AMPAR function (34, 43, 56, 57, 84). A more recent study showed that both PFC and medio-dorsal thalamic (MDT) NAcs inputs exhibit mGluRI-LTD that requires different one limitation of our study is that we did not differentiate D1 or D2 MSNs, nor mGluRI subtypes, we observed robust mGluRI-LTD at mPFC, vHipp, and BLA inputs to NAcs MSNs, and a loss of LTD at mPFC and vHipp afferents after chronic Δ^9-THC. Therefore, together these data suggest that mGluRI-LTD differentially occurs at a subset of NAcs afferents (BLA, mPFC, vHipp, and MDT), and that mGluRI-LTD is disrupted by chronic exposure to Δ^9-THC at all but the BLA inputs. The large increase in vHipp pathway strength after chronic Δ^9-THC would likely enhance its influence on NAc output, whereas the impaired LTD would render it resistant to subsequent dampening. Given the hypothesized role for vHipp → NAcs inputs in mediating the contextual salience of drug-paired environmental stimuli (73), we predict greater vulnerability to these cues in long-term cannabis users.

The changes in synaptic strength we observe in these NAc afferents may result from the ability of chronic Δ^9-THC to cause CB1R downregulation, desensitization, and tolerance (43, 85). However, this implies a role for endocannabinoids in tonically regulating NAc afferents that is disrupted by chronic Δ^9-THC. Our data argue against this possibility because changes in the strength of NAcs inputs were not observed following chronic AM251 treatment alone (Fig. 1C–F), and previous studies do not show tonic modulation of NAc synapses by endocannabinoids. Therefore, we speculate that more widespread changes in upstream brain networks by chronic Δ^9-THC contributes to the rebalancing of NAc afferents that we observe.

Implications for cannabis involvement in CUD and psychiatric symptoms

The symptoms defining CUD include altered mood, attention, motivation, cognition, and self-control. Extensive preclinical and human evidence supports a role for PFC in these processes, as well as in compulsive drug seeking (86, 87). The extensive connections of PFC with subcortical structures mediating motivated behavior has inspired hypotheses defining the PFC as a “top-down” inhibitor of behavior leading to undesired outcomes (86, 88, 89). Moreover, loss of control of subcortical circuits by PFC is hypothesized to underlie a shift from purposeful control of action to more habitual, automatic behaviors, regulated by

emotion and arousal (88). In our study, long-term exposure to Δ^9-THC substantially weakened mPFC influence on the NAcs and strengthened BLA and vHipp inputs. We hypothesize that this shift in control of the NAc away from the PFC is involved in the cognitive and emotional dysregulation found in CUD. Moreover, as there is also strong evidence for involvement of corticolimbic circuitry in psychotic disorders such as schizophrenia (80, 90, 91), and there is an elevated risk for psychotic disorders in heavy cannabis users (16, 18, 20, 92), this disrupted balance of NAc afferents by Δ^9-THC may contribute to the symptomology of these disorders in the cannabis using population.

Supplementary Material

Refer to Web version on PubMed Central for supplementary material.

Acknowledgements

This work is supported by the National Institutes of Health and the NIDA Intramural Research

Program. We thank Dr. Alex Hoffman for a critical reading of the manuscript.

References

1. Thomas MJ, Kalivas PW, Shaham Y (2008): Neuroplasticity in the mesolimbic dopamine system and cocaine addiction. British Journal of Pharmacology. 154:327–342. [PubMed: 18345022]
2. Volkow Nora D, Morales M (2015): The Brain on Drugs: From Reward to Addiction. Cell. 162:712–725. [PubMed: 26276628]
3. Mogenson GJ, Jones DL, Yim CY (1980): From motivation to action: functional interface between the limbic system and the motor system. Prog Neurobiol. 14:69–97. [PubMed: 6999537]
4. Pierce RC, Wolf ME (2013): Psychostimulant-Induced Neuroadaptations in Nucleus Accumbens AMPA Receptor Transmission. Cold Spring Harbor Perspectives in Medicine. 3.
5. Floresco SB (2015): The nucleus accumbens: an interface between cognition, emotion, and action. Annu Rev Psychol. 66:25–52. [PubMed: 25251489]
6. Kauer JA, Malenka RC (2007): Synaptic plasticity and addiction. Nat Rev Neurosci. 8:844–858. [PubMed: 17948030]
7. Luscher C, Malenka RC (2011): Drug-evoked synaptic plasticity in addiction: from molecular changes to circuit remodeling. Neuron. 69:650–663. [PubMed: 21338877]
8. Wolf ME (2016): Synaptic mechanisms underlying persistent cocaine craving. Nat Rev Neurosci. 17:351–365. [PubMed: 27150400]
9. Wolf ME, Ferrario CR (2010): AMPA receptor plasticity in the nucleus accumbens after repeated exposure to cocaine. Neurosci Biobehav Rev. 35:185–211. [PubMed: 20109488]
10. Boudreau AC, Wolf ME (2005): Behavioral sensitization to cocaine is associated with increased AMPA receptor surface expression in the nucleus accumbens. J Neurosci. 25:9144–9151. [PubMed: 16207873]
11. Kourrich S, Rothwell PE, Klug JR, Thomas MJ (2007): Cocaine Experience Controls Bidirectional Synaptic Plasticity in the Nucleus Accumbens. Journal of Neuroscience. 27:7921–7928. [PubMed: 17652583]
12. Terrier J, Lüscher C, Pascoli V (2015): Cell-Type Specific Insertion of GluA2-Lacking AMPARs with Cocaine Exposure Leading to Sensitization, Cue-Induced Seeking, and Incubation of Craving. Neuropsychopharmacology. 41:1779. [PubMed: 26585289]
13. United Nations Office on Drugs and Crime WDR (2017): United Nations Office on Drugs and Crime. World Drug Report 2017.

14. Di Forti M, Quattrone D, Freeman TP, Tripoli G, Gayer-Anderson C, Quigley H, et al. (2019): The contribution of cannabis use to variation in the incidence of psychotic disorder across Europe (EU-GEI): a multicentre case-control study. The Lancet Psychiatry. 6:427–436. [PubMed: 30902669]
15. Arseneault L, Cannon M, Poulton R, Murray R, Caspi A, Moffitt TE (2002): Cannabis use in adolescence and risk for adult psychosis: longitudinal prospective study. BMJ. 325:1212–1213. [PubMed: 12446537]
16. Lupica CR, Hu Y, Devinsky O, Hoffman AF (2017): Cannabinoids as hippocampal network administrators. Neuropharmacology. 124:25–37. [PubMed: 28392266]
17. National Academies of Sciences E, Medicine (2017): The Health Effects of Cannabis and Cannabinoids: The Current State of Evidence and Recommendations for Research. Washington, DC: The National Academies Press.
18. Di Forti M, Marconi A, Carra E, Fraietta S, Trotta A, Bonomo M, et al. (2015): Proportion of patients in south London with first-episode psychosis attributable to use of high potency cannabis: a case-control study. The Lancet Psychiatry. 2:233–238. [PubMed: 26359901]
19. Chandra S, Radwan MM, Majumdar CG, Church JC, Freeman TP, ElSohly MA (2019): New trends in cannabis potency in USA and Europe during the last decade (2008–2017). European Archives of Psychiatry and Clinical Neuroscience. 269:5–15. [PubMed: 30671616]
20. Broyd SJ, van Hell HH, Beale C, Yücel M, Solowij N (2016): Acute and Chronic Effects of Cannabinoids on Human Cognition—A Systematic Review. Biological Psychiatry. 79:557–567. [PubMed: 26858214]
21. Fischer AS, Whitfield-Gabrieli S, Roth RM, Brunette MF, Green AI (2014): Impaired functional connectivity of brain reward circuitry in patients with schizophrenia and cannabis use disorder: Effects of cannabis and THC. Schizophrenia Research. 158:176–182. [PubMed: 25037524]
22. Koob GF, Volkow ND (2016): Neurobiology of addiction: a neurocircuitry analysis. The Lancet Psychiatry. 3:760–773. [PubMed: 27475769]
23. Volkow ND, Wang G-J, Telang F, Fowler JS, Alexoff D, Logan J, et al. (2014): Decreased dopamine brain reactivity in marijuana abusers is associated with negative emotionality and addiction severity. Proceedings of the National Academy of Sciences. 111:E3149–E3156.
24. Devane WA, Dysarz FA, Johnson MR, Melvin LS, Howlett AC (1988): Determination and characterization of a cannabinoid receptor in rat brain. Molecular Pharmacology. 34:605–613. [PubMed: 2848184]
25. Bidaut-Russell M, Devane WA, Howlett AC (1990): Cannabinoid receptors and modulation of cyclic AMP accumulation in the rat brain. J Neurochem. 55:21–26. [PubMed: 2162376]
26. Laaris N, Good CH, Lupica CR (2010): Delta9-tetrahydrocannabinol is a full agonist at CB1 receptors on GABA neuron axon terminals in the hippocampus. Neuropharmacology. 59:121–127. [PubMed: 20417220]
27. Chen JP, Paredes W, Li J, Smith D, Lowinson J, Gardner EL (1990): Delta 9-tetrahydrocannabinol produces naloxone-blockable enhancement of presynaptic basal dopamine efflux in nucleus accumbens of conscious, freely-moving rats as measured by intracerebral microdialysis. Psychopharmacology (Berl). 102:156–162. [PubMed: 2177204]
28. Tanda G, Pontieri FE, Di Chiara G (1997): Cannabinoid and heroin activation of mesolimbic dopamine transmission by a common μ_1 opioid receptor mechanism. Science. 276:2048–2050. [PubMed: 9197269]
29. Wise RA, Bozarth MA (1985): Brain mechanisms of drug reward and euphoria. Psychiatr Med. 3:445–460. [PubMed: 2893431]
30. Yamaguchi T, Wang HL, Li X, Ng TH, Morales M (2011): Mesocorticolimbic Glutamatergic Pathway. The Journal of Neuroscience. 31:8476–8490. [PubMed: 21653852]
31. Zhang S, Qi J, Li X, Wang HL, Britt JP, Hoffman AF, et al. (2015): Dopaminergic and glutamatergic microdomains in a subset of rodent mesoaccumbens axons. Nat Neurosci. 18:386–392. [PubMed: 25664911]
32. Tecuapetla F, Patel JC, Xenias H, English D, Tadros I, Shah F, et al. (2010): Glutamatergic Signaling by Mesolimbic Dopamine Neurons in the Nucleus Accumbens. The Journal of Neuroscience. 30:7105–7110. [PubMed: 20484653]

33. Stuber GD, Hnasko TS, Britt JP, Edwards RH, Bonci A (2010): Dopaminergic Terminals in the Nucleus Accumbens But Not the Dorsal Striatum Corelease Glutamate. The Journal of Neuroscience. 30:8229–8233. [PubMed: 20554874]
34. Loweth JA, Scheyer AF, Milovanovic M, LaCrosse AL, Flores-Barrera E, Werner CT, et al. (2014): Synaptic depression via mGluR1 positive allosteric modulation suppresses cue-induced cocaine craving. Nat Neurosci. 17:73–80. [PubMed: 24270186]
35. Verdejo-Garcia A, Contreras-Rodriguez O, Fonseca F, Cuenca A, Soriano-Mas C, Rodriguez J, et al. (2014): Functional alteration in frontolimbic systems relevant to moral judgment in cocaine-dependent subjects. Addict Biol. 19:272–281. [PubMed: 22784032]
36. Goto Y, O'Donnell P (2004): Prefrontal lesion reverses abnormal mesoaccumbens response in an animal model of schizophrenia. Biol Psychiatry. 55:172–176. [PubMed: 14732597]
37. Manza P, Tomasi D, Volkow ND (2018): Subcortical Local Functional Hyperconnectivity in Cannabis Dependence. Biol Psychiatry Cogn Neurosci Neuroimaging. 3:285–293. [PubMed: 29486870]
38. Crean RD, Tapert SF, Minassian A, Macdonald K, Crane NA, Mason BJ (2011): Effects of chronic, heavy cannabis use on executive functions. J Addict Med. 5:9–15. [PubMed: 21643485]
39. Mizrahi R, Watts JJ, Tseng KY (2017): Mechanisms contributing to cognitive deficits in cannabis users. Neuropharmacology. 124:84–88. [PubMed: 28414051]
40. Batalla A, Bhattacharyya S, Yücel M, Fusar-Poli P, Crippa JA, Nogué S, et al. (2013): Structural and Functional Imaging Studies in Chronic Cannabis Users: A Systematic Review of Adolescent and Adult Findings. PLOS ONE. 8:e55821. [PubMed: 23390554]
41. Lorenzetti V, Solowij N, Yücel M (2016): The Role of Cannabinoids in Neuroanatomic Alterations in Cannabis Users. Biological Psychiatry. 79:e17–e31. [PubMed: 26858212]
42. Mato S, Chevaleyre V, Robbe D, Pazos A, Castillo PE, Manzoni OJ (2004): A single in-vivo exposure to Delta9THC blocks endocannabinoid-mediated synaptic plasticity. Nat Neurosci. 7:585–586. [PubMed: 15146190]
43. Hoffman AF, Oz M, Caulder T, Lupica CR (2003): Functional tolerance and blockade of long-term depression at synapses in the nucleus accumbens after chronic cannabinoid exposure. J Neurosci. 23:4815–4820. [PubMed: 12832502]
44. Ting JT, Lee BR, Chong P, Soler-Llavina G, Cobbs C, Koch C, et al. (2018): Preparation of Acute Brain Slices Using an Optimized N-Methyl-D-glucamine Protective Recovery Method. J Vis Exp.
45. Huang YH, Ishikawa M, Lee BR, Nakanishi N, Schlüter OM, Dong Y (2011): Searching for Presynaptic NMDA Receptors in the Nucleus Accumbens. The Journal of Neuroscience. 31:18453. [PubMed: 22171047]
46. Suska A, Lee BR, Huang YH, Dong Y, Schlüter OM (2013): Selective presynaptic enhancement of the prefrontal cortex to nucleus accumbens pathway by cocaine. Proceedings of the National Academy of Sciences. 110:713.
47. Hessler NA, Shirke AM, Malinow R (1993): The probability of transmitter release at a mammalian central synapse. Nature. 366:569–572. [PubMed: 7902955]
48. Huang EP, Stevens CF (1997): Estimating the distribution of synaptic reliabilities. J Neurophysiol. 78:2870–2880. [PubMed: 9405507]
49. Hollmann M, Hartley M, Heinemann S (1991): Ca2+ permeability of KA-AMPA--gated glutamate receptor channels depends on subunit composition. Science. 252:851–853. [PubMed: 1709304]
50. Isaac JTR, Ashby MC, McBain CJ (2007): The Role of the GluR2 Subunit in AMPA Receptor Function and Synaptic Plasticity. Neuron. 54:859–871. [PubMed: 17582328]
51. Conrad KL, Tseng KY, Uejima JL, Reimers JM, Heng LJ, Shaham Y, et al. (2008): Formation of accumbens GluR2-lacking AMPA receptors mediates incubation of cocaine craving. Nature. 454:118–121. [PubMed: 18500330]
52. Werner CT, Murray CH, Reimers JM, Chauhan NM, Woo KKY, Molla HM, et al. (2017): Trafficking of calcium-permeable and calcium-impermeable AMPA receptors in nucleus accumbens medium spiny neurons co-cultured with prefrontal cortex neurons. Neuropharmacology. 116:224–232. [PubMed: 27993521]

53. Lee BR, Ma Y-Y, Huang YH, Wang X, Otaka M, Ishikawa M, et al. (2013): Maturation of silent synapses in amygdala-accumbens projection contributes to incubation of cocaine craving. Nat Neurosci. 16:1644–1651. [PubMed: 24077564]
54. Bellone C, Luscher C (2006): Cocaine triggered AMPA receptor redistribution is reversed in vivo by mGluR-dependent long-term depression. Nat Neurosci. 9:636–641. [PubMed: 16582902]
55. Koike M, Iino M, Ozawa S (1997): Blocking effect of 1-naphthyl acetyl spermine on Ca2+-permeable AMPA receptors in cultured rat hippocampal neurons. Neuroscience Research. 29:27–36. [PubMed: 9293490]
56. Robbe D, Kopf M, Remaury A, Bockaert J, Manzoni OJ (2002): Endogenous cannabinoids mediate long-term synaptic depression in the nucleus accumbens. Proc Natl Acad Sci U S A. 99:8384–8388. [PubMed: 12060781]
57. Ma YY, Wang X, Huang Y, Marie H, Nestler EJ, Schluter OM, et al. (2016): Re-silencing of silent synapses unmasks anti-relapse effects of environmental enrichment. Proc Natl Acad Sci U S A. 113:5089–5094. [PubMed: 27091967]
58. Turner BD, Rook JM, Lindsley CW, Conn PJ, Grueter BA (2018): mGlu1 and mGlu5 modulate distinct excitatory inputs to the nucleus accumbens shell. Neuropsychopharmacology. 43:2075–2082. [PubMed: 29654259]
59. Pascoli V, Terrier J, Espallergues J, Valjent E, O'Connor EC, Lüscher C (2014): Contrasting forms of cocaine-evoked plasticity control components of relapse. Nature. 509:459. [PubMed: 24848058]
60. De Petrocellis L, Di Marzo V (2010): Non-CB1, Non-CB2 Receptors for Endocannabinoids, Plant Cannabinoids, and Synthetic Cannabimimetics: Focus on G-protein-coupled Receptors and Transient Receptor Potential Channels. Journal of Neuroimmune Pharmacology. 5:103–121. [PubMed: 19847654]
61. Nguyen JD, Aarde SM, Vandewater SA, Grant Y, Stouffer DG, Parsons LH, et al. (2016): Inhaled delivery of Delta(9)-tetrahydrocannabinol (THC) to rats by e-cigarette vapor technology. Neuropharmacology. 109:112–120. [PubMed: 27256501]
62. Huestis MA, Henningfield JE, Cone EJ (1992): Blood cannabinoids. I. Absorption of THC and formation of 11-OH-THC and THCCOOH during and after smoking marijuana. J Anal Toxicol. 16:276–282. [PubMed: 1338215]
63. Hoffman AF, Oz M, Yang R, Lichtman AH, Lupica CR (2007): Opposing actions of chronic Δ9-tetrahydrocannabinol and cannabinoid antagonists on hippocampal long-term potentiation. Learn Mem. 14:63–74. [PubMed: 17202425]
64. Bellone C, Luscher C (2005): mGluRs induce a long-term depression in the ventral tegmental area that involves a switch of the subunit composition of AMPA receptors. Eur J Neurosci. 21:1280–1288. [PubMed: 15813937]
65. Argilli E, Sibley DR, Malenka RC, England PM, Bonci A (2008): Mechanism and time course of cocaine-induced long-term potentiation in the ventral tegmental area. J Neurosci. 28:9092–9100. [PubMed: 18784289]
66. Ungless MA, Whistler JL, Malenka RC, Bonci A (2001): Single cocaine exposure in vivo induces long-term potentiation in dopamine neurons. Nature. 411:583–587. [PubMed: 11385572]
67. Bredt DS, Nicoll RA (2003): AMPA receptor trafficking at excitatory synapses. Neuron. 40:361–79. [PubMed: 14556714]
68. Koya E, Cruz FC, Ator R, Golden SA, Hoffman AF, Lupica CR, et al. (2012): Silent synapses in selectively activated nucleus accumbens neurons following cocaine sensitization. Nat Neurosci. 15:1556–1562. [PubMed: 23023294]
69. Britt Jonathan P, Benaliouad F, McDevitt Ross A, Stuber Garret D, Wise Roy A, Bonci A (2012): Synaptic and Behavioral Profile of Multiple Glutamatergic Inputs to the Nucleus Accumbens. Neuron. 76:790–803. [PubMed: 23177963]
70. Floresco SB, Todd CL, Grace AA (2001): Glutamatergic afferents from the hippocampus to the nucleus accumbens regulate activity of ventral tegmental area dopamine neurons. J Neurosci. 21:4915–4922. [PubMed: 11425919]
71. Legault M, Rompre PP, Wise RA (2000): Chemical stimulation of the ventral hippocampus elevates nucleus accumbens dopamine by activating dopaminergic neurons of the ventral tegmental area. J Neurosci. 20:1635–1642. [PubMed: 10662853]

72. Loureiro M, Renard J, Zunder J, Laviolette SR (2015): Hippocampal cannabinoid transmission modulates dopamine neuron activity: impact on rewarding memory formation and social interaction. Neuropsychopharmacology. 40:1436–1447. [PubMed: 25510937]
73. Everitt BJ, Robbins TW (2005): Neural systems of reinforcement for drug addiction: from actions to habits to compulsion. Nature Neuroscience. 8:1481. [PubMed: 16251991]
74. Sulzer D, Joyce MP, Lin L, Geldwert D, Haber SN, Hattori T, et al. (1998): Dopamine neurons make glutamatergic synapses in vitro. J Neurosci. 18:4588–4602. [PubMed: 9614234]
75. Bourque MJ, Trudeau LE (2000): GDNF enhances the synaptic efficacy of dopaminergic neurons in culture. Eur J Neurosci. 12:3172–3180. [PubMed: 10998101]
76. Wang DV, Viereckel T, Zell V, Konradsson-Geuken Å, Broker CJ, Talishinsky A, et al. (2017): Disrupting Glutamate Co-transmission Does Not Affect Acquisition of Conditioned Behavior Reinforced by Dopamine Neuron Activation. Cell Reports. 18:2584–2591. [PubMed: 28297663]
77. Turrigiano GG, Nelson SB (2004): Homeostatic plasticity in the developing nervous system. Nat Rev Neurosci. 5:97–107. [PubMed: 14735113]
78. O'Donnell P, Greene J, Pabello N, Lewis BL, Grace AA (1999): Modulation of cell firing in the nucleus accumbens. Ann N Y Acad Sci. 877:157–175. [PubMed: 10415649]
79. O'Donnell P, Grace AA (1995): Synaptic interactions among excitatory afferents to nucleus accumbens neurons: hippocampal gating of prefrontal cortical input. J Neurosci. 15:3622–3639. [PubMed: 7751934]
80. Goto Y, Grace AA (2008): Limbic and cortical information processing in the nucleus accumbens. Trends Neurosci. 31:552–558. [PubMed: 18786735]
81. Sesack SR, Grace AA (2010): Cortico-Basal Ganglia reward network: microcircuitry. Neuropsychopharmacology. 35:27–47. [PubMed: 19675534]
82. French SJ, Totterdell S (2002): Hippocampal and prefrontal cortical inputs monosynaptically converge with individual projection neurons of the nucleus accumbens. J Comp Neurol. 446:151–165. [PubMed: 11932933]
83. Finch DM (1996): Neurophysiology of converging synaptic inputs from the rat prefrontal cortex, amygdala, midline thalamus, and hippocampal formation onto single neurons of the caudate/putamen and nucleus accumbens. Hippocampus. 6:495–512. [PubMed: 8953303]
84. McCutcheon JE, Loweth JA, Ford KA, Marinelli M, Wolf ME, Tseng KY (2011): Group I mGluR Activation Reverses Cocaine-Induced Accumulation of Calcium-Permeable AMPA Receptors in Nucleus Accumbens Synapses via a Protein Kinase C-Dependent Mechanism. The Journal of Neuroscience. 31:14536–14541. [PubMed: 21994370]
85. Sim-Selley LJ (2003): Regulation of cannabinoid CB1 receptors in the central nervous system by chronic cannabinoids. Crit Rev Neurobiol. 15:91–119. [PubMed: 14977366]
86. Jentsch JD, Taylor JR (1999): Impulsivity resulting from frontostriatal dysfunction in drug abuse: implications for the control of behavior by reward-related stimuli. Psychopharmacology. 146:373–390. [PubMed: 10550488]
87. Goldstein RZ, Volkow ND (2011): Dysfunction of the prefrontal cortex in addiction: neuroimaging findings and clinical implications. Nature Reviews Neuroscience. 12:652. [PubMed: 22011681]
88. Belin D, Belin-Rauscent A, Murray JE, Everitt BJ (2013): Addiction: failure of control over maladaptive incentive habits. Current Opinion in Neurobiology. 23:564–572. [PubMed: 23452942]
89. Everitt Barry J, Belin D, Economidou D, Pelloux Y, Dalley Jeffrey W, Robbins Trevor W (2008): Neural mechanisms underlying the vulnerability to develop compulsive drug-seeking habits and addiction. Philosophical Transactions of the Royal Society B: Biological Sciences. 363:3125–3135.
90. Winton-Brown T, Schmidt A, Roiser JP, Howes OD, Egerton A, Fusar-Poli P, et al. (2017): Altered activation and connectivity in a hippocampal–basal ganglia–midbrain circuit during salience processing in subjects at ultra high risk for psychosis. Translational Psychiatry. 7:e1245. [PubMed: 28972591]
91. Floresco SB, Zhang Y, Enomoto T (2009): Neural circuits subserving behavioral flexibility and their relevance to schizophrenia. Behavioural Brain Research. 204:396–409. [PubMed: 19110006]

92. Moore THM, Zammit S, Lingford-Hughes A, Barnes TRE, Jones PB, Burke M, et al. (2007): Cannabis use and risk of psychotic or affective mental health outcomes: a systematic review. The Lancet. 370:319–328.

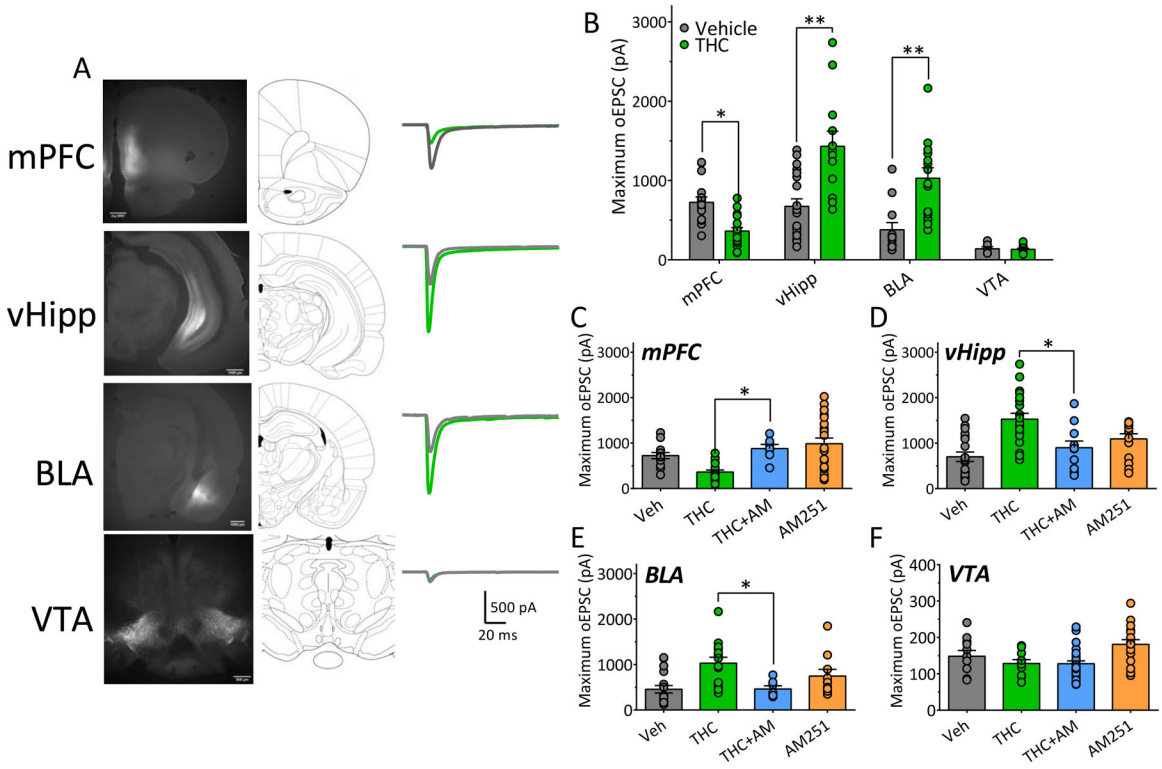

Figure 1. Pathway-specific alteration of NAcs excitatory afferent pathways by chronic Δ^9-THC

A. Representative fluorescence images and corresponding rat brain diagrams of coronal brain slices showing injection sites of ChR2 viruses in brain regions projecting to the NAcs (mPFC, medial prefrontal cortex; vHipp, ventral hippocampus; BLA, basolateral amygdala; VTA, ventral tegmental area). At right are representative averages of maximum excitatory postsynaptic current traces (oEPSCs) recorded in NAcs neurons and evoked by 473nm light-activation of ChR2, expressed by afferent axon terminals originating in the brain areas at left. Gray waveforms were obtained from rats treated with vehicle, whereas green traces are those obtained from animals chronically treated with Δ^9-THC. **B**. Mean maximum oEPSCs in NAcs neurons that were evoked by light-stimulation of ChR2 expressed in axons originating in each of the brain regions injected with ChR2-AAV. oEPSCs recorded from both chronic vehicle- and Δ^9-THC-injected rats are shown (Two-way ANOVA interaction, $F_{3,100} = 16.2$, $p < 0.0001$; Bonferroni post-hoc comparisons, * = $p < 0.01$, ** = $p < 0.0001$). **C.** Maximal light-evoked oEPSCs recorded in the NAcs of rats injected with ChR2 virus in the mPFC after chronic vehicle, Δ^9-THC, Δ^9-THC preceded by injection of the CB1 antagonist AM251, or AM251 alone (One-way ANOVA, $F_{3,59} = 8.4$, $p < 0.0001$; Holm-Sidak post-hoc comparison of THC vs. THC+AM251, * = $p = 0.026$). **D.** Maximal vHipp-evoked oEPSCs recorded after chronic vehicle, Δ^9-THC, Δ^9-THC preceded by injection of the CB1 antagonist AM251, or AM251 alone (One-way ANOVA, $F_{3,60} = 9.8$, $p < 0.0001$; Holm-Sidak post-hoc comparisons of THC vs. THC+AM251, $p = 0.006$). **E.** Maximal BLA-evoked oEPSCs recorded after chronic vehicle, Δ^9-THC, Δ^9-THC preceded by injection of the CB1 antagonist AM251, or AM251 alone (One-way ANOVA, $F_{3,45} = 6.1$, $p < 0.01$; Holm-Sidak post-hoc comparison of THC vs. THC+AM251, * = $p = 0.021$). **F.** Maximal VTA-evoked oEPSCs recorded after chronic vehicle, Δ^9-THC, Δ^9-THC preceded by

injection of the CB1 antagonist AM251, or AM251 alone (One-way ANOVA, $F_{3,62} = 1.02$, $p = 0.37$). Data in **C-F** illustrate that the effect of chronic Δ^9-THC was significantly prevented in mPFC, vHipp, and BLA projections to the NAcs when each injection was preceded by an injection of AM251. Numbers of neurons recorded from number of rats (n/R) in each experiment = **A.** mPFC, Veh: 16/11, THC: 18/7; vHipp, Veh: 19/8, THC: 12/7; BLA, Veh: 12, THC: 14; VTA, Veh: 6, THC: 11. **B.** mPFC, Veh: 16/11, THC: 18/7; vHipp, Veh: 19/8, THC: 12/7; BLA, Veh: 12, THC: 14; VTA, Veh: 6, THC: 11. **C.** mPFC, Veh: 16/11, THC: 18/7, THC+AM: 7/5, AM251: 21/6. **D.** vHipp, Veh: 19/8, THC: 20/7, THC+AM: 11/4, AM251: 14/5. **E.** BLA, Veh: 18/7, THC: 14/6, THC+AM: 7/4, AM251: 10/5. **F.** VTA: Veh: 11/6, THC: 10/6, THC+AM: 32/8, AM251: 17/7.

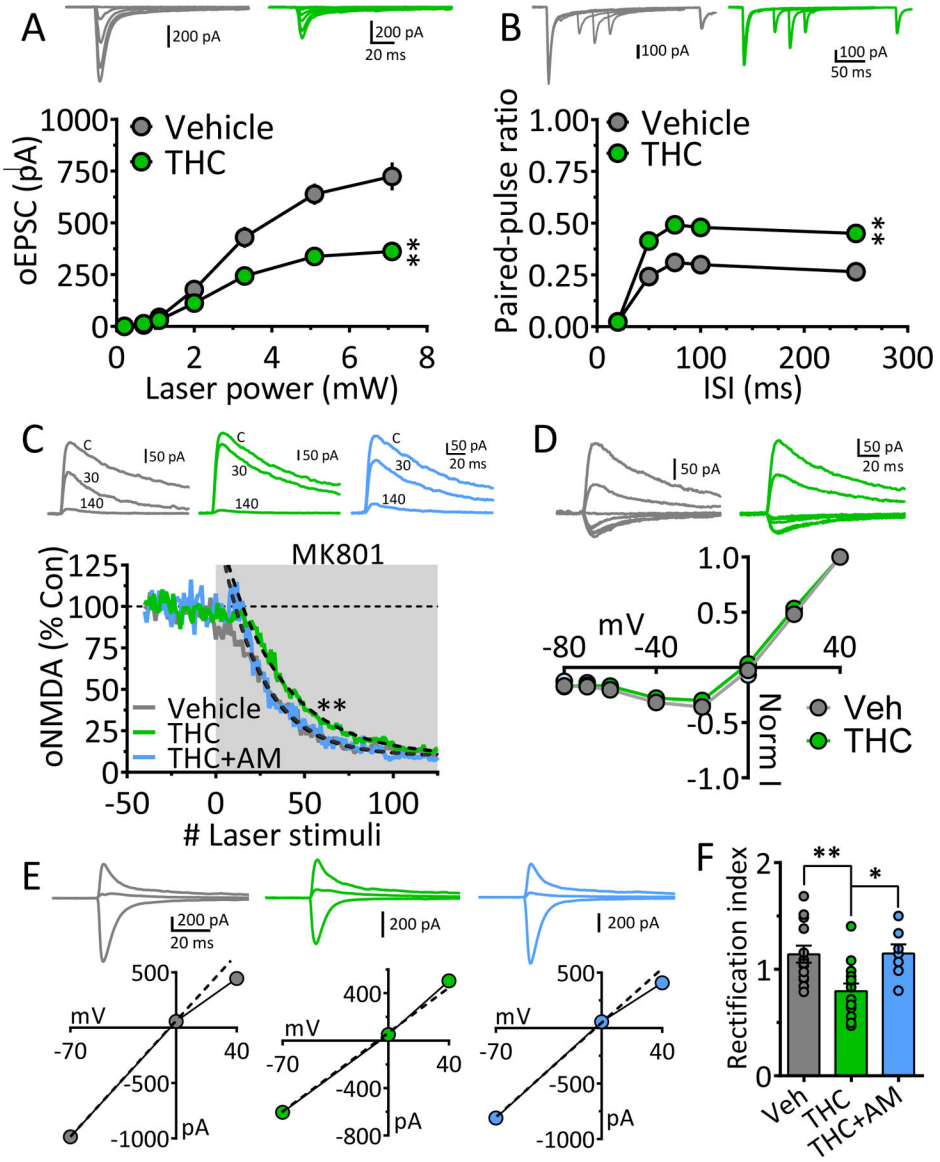

Figure 2. Mechanisms underlying weakened mPFC glutamatergic input to NAcs following chronic Δ^9-THC.

A. Input-output (I-O) curves showing relationship between laser power, activating ChR2 in mPFC axons projecting to NAcs, and oEPSC amplitudes after chronic vehicle or Δ^9-THC injections. Representative mean oEPSCs are shown at 5 laser intensities in neurons from vehicle (gray traces) and Δ^9-THC-injected (green traces) rats. The strength of mPFC glutamate input to NAcs neurons was significantly smaller following chronic Δ^9-THC (** = $F_{18,342} = 9.2$, $p < 0.0001$, intensity x treatment interaction, two-way repeated measures ANOVA).**B.** Mean paired-pulse ratios (PPR) of mPFC-evoked oEPSCs at different inter-stimulus (laser pulse) intervals (ISI) in NAc neurons from chronic Δ^9-THC- and vehicle injected rats. Mean representative traces from individual cells in both groups are shown above. The PPR was significantly increased by chronic Δ^9-THC treatment (** = $F_{12,208} = 3.9$, $p < 0.0001$, ISI x treatment interaction, two-way repeated measures ANOVA). Note that paired oEPSCs overlapped at the 20 ms ISI, thereby yielding a ratio = 0. **C.** The rate of the

progressive, activity-dependent, block of ChR2-evoked NMDA receptor oEPSCs by MK801, is significantly slower following chronic Δ^9-THC in the mPFC → NAcs pathway (time-constant of oNMDA current reduction in MK801: chronic vehicle = 23.4 stimuli, 95% confidence interval = 22.2 – 24.5 stimuli, n = 8, gray; chronic Δ^9-THC = 32.5 stimuli, 95% confidence interval = 30.9 – 34.2 stimuli, n = 8, green), and this was prevented by co-injection with the cannabinoid antagonist AM251 (chronic Δ^9-THC + AM251 = 24.0 stimuli, 95% confidence interval = 22.8 – 25.4 stimuli, n = 4, blue). Exponential decay time constants (τ) were obtained by curve fitting (dashed lines). Representative oNMDA waveforms from each group obtained before MK801 application (control, C), and at 30 and 140 stimuli are shown above. Note the smaller reduction of the oNMDA current at 30 stimuli in the cell from the chronic Δ^9-THC treated animal compared to the other groups. Recordings were performed in the presence of DNQX, a kainate/AMPA receptor antagonist, and picrotoxin, a $GABA_A$ Cl^- channel blocker. **D.** Lack of chronic Δ^9-THC effect on the voltage-dependence of oNMDA currents. Representative mean traces obtained from chronic vehicle (gray) and Δ^9-THC-treated (green) cells are shown above. **E.** Chronic Δ^9-THC causes a reduction in inward rectification of ChR2-evoked AMPA receptor-mediated synaptic currents at mPFC → NAcs synapses. Shown are representative current-voltage (I-V) relationships and mean waveforms of AMPA oEPSCs evoked by activation of ChR2 in the mPFC → NAcs pathway at 3 different membrane voltages (Vm = −70, 0, and +40) from each group (chronic vehicle, gray, chronic Δ^9-THC, green, and chronic Δ^9-THC + AM251, blue). A hypothetical slope = 1.0 is indicated by a dashed line. **F.** Mean rectification index (RI = absolute AMPA current measured at −70 mV divided by that measured at +40 mV) for all cells in each group. The cells from chronic Δ^9-THC-treated animals showed a significant reduction in rectification index compared to chronic vehicle-, or chronic Δ^9-THC + AM251-treated rats ($F_{3,44} = 5.6$, $p < 0.001$, one-way ANOVA, ** = $p < 0.001$, * = $p < 0.05$, Holm-Sidak post-hoc comparison, respectively). Number of neurons/number of rats: **A.** Veh: 16/11, THC: 18/ 6 **B.** Veh: 12/11, THC: 15/6. **C.** Veh: 8/6, THC: 8/5, THC+AM: 4/4. **D.** Veh: 9/6, THC: 7/5. **F.** Veh: 13/6, THC: 13/5, THC+AM: 7/4.

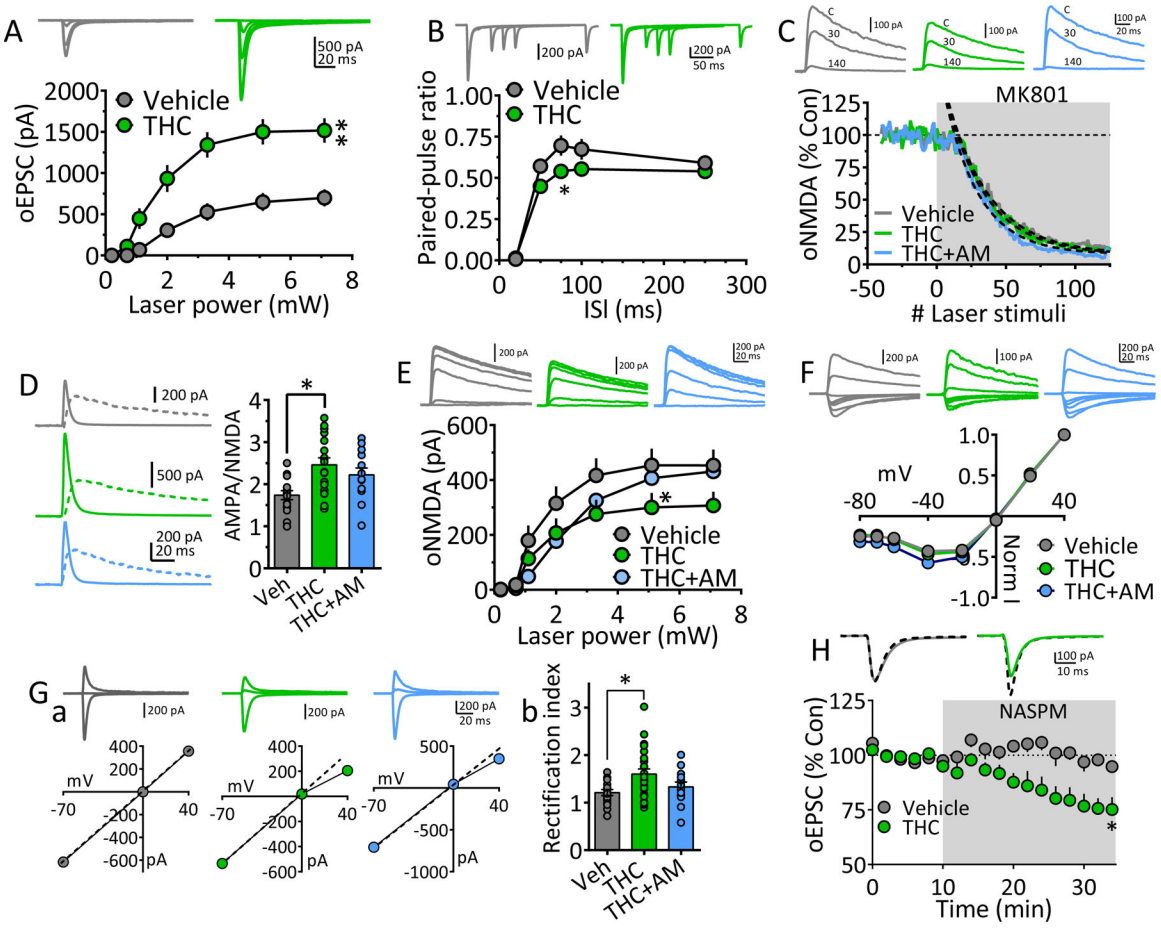

Figure 3. Mechanisms underlying strengthened vHipp glutamatergic input to NAcs following chronic Δ^9-THC.

A. oEPSC I-O curves evoked by ChR2 activation of vHipp axons projecting to NAcs, after chronic vehicle or Δ^9-THC injections. Representative mean oEPSCs are shown at 5 laser intensities in neurons from vehicle (gray traces) and Δ^9-THC-injected (green traces) rats. The strength of vHipp glutamate input to NAcs neurons was significantly increased following chronic Δ^9-THC (** = $F_{18,336} = 5.6$, $p < 0.0001$, intensity x treatment interaction, two-way repeated measures ANOVA). **B.** Mean PPR of vHipp-evoked oEPSCs at different inter-laser pulse intervals (ISI) in NAc neurons from chronic Δ^9-THC- and vehicle injected rats. Mean representative traces from individual cells in both groups are shown above. The PPR was significantly decreased by chronic Δ^9-THC treatment only at the 75ms ISI (* = $F_{4,100} = 4.5$, $p = 0.002$, ISI x treatment interaction, two-way repeated measures ANOVA, $p = 0.016$, Holm-Sidak post-hoc comparison). Note that paired oEPSCs overlapped at the 20 ms ISI, thereby yielding a ratio = 0. **C.** The rate of block of ChR2-evoked NMDA receptor oEPSCs by MK801, was not significantly altered by chronic Δ^9-THC in the vHipp → NAcs pathway (time-constant of oNMDA current block by MK801: chronic vehicle = 30.7 stimuli, 95% confidence interval = 29.4 – 32.2.5 stimuli, n = 8, gray; chronic Δ^9-THC = 28.8 stimuli, 95% confidence interval = 27.5 – 30.2 stimuli, n = 8, green; chronic Δ^9-THC + AM251 = 25.1 stimuli, 95% confidence interval = 23.9 – 26.3 stimuli, n = 4, blue). Exponential decay time constants (τ) were obtained by best fit (dashed lines). Representative oNMDA

waveforms from each group obtained before MK801 application (control, C), and at 30 and 140 stimuli are shown above. **D.** AMPA/NMDA ratios show potentiated transmission at vHipp → NAcs synapses. Left, representative mean waveforms of laser-evoked oEPSCs collected at −70 mV (solid line) and +40 mV (dashed line) holding potentials from chronic vehicle (gray), chronic Δ^9-THC (green), or chronic Δ^9-THC + AM251 (blue) groups. AMPA/NMDA = peak AMPA response at −70 mV divided by the peak NMDA response at +40 mV. Right, AMPA/NMDA ratio group means (± s.e.m.). * = $p < 0.01$, $F_{3,62} = 5.28$, 1-way ANOVA and Holm-Sidak post-hoc comparison). **E.** I-O curves of vHipp ChR2-evoked oNMDA currents in neurons from chronic vehicle, chronic Δ^9-THC, and chronic Δ^9-THC + AM251 treated rats. Representative mean oNMDA wave forms are shown above for each condition. oNMDA currents were significantly smaller following chronic Δ^9-THC at only one laser intensity ($F_{12,204} = 2.062$, drug x power interaction, $p < 0.05$, 2-way repeated measures ANOVA; * = $p < 0.05$, Holm-Sidak's post-hoc test). **F.** Lack of chronic Δ^9-THC effect on the voltage-dependence of oNMDA currents. Representative mean traces from cells in chronic vehicle (gray), Δ^9-THC-treated (green), and Δ^9-THC + AM251 groups are shown above. **G.** Chronic Δ^9-THC increased inward rectification of ChR2-evoked AMPA receptor oEPSCs at vHipp →NAcs synapses. **Ga.** Representative I-V relationships and mean AMPA oEPSCs evoked by ChR2 in the vHipp → NAcs pathway at holding potentials of −70, 0, and +40 from each of the 3 groups (chronic vehicle, gray, chronic Δ^9-THC, green, and chronic Δ^9-THC + AM251, blue). A hypothetical slope = 1.0 is indicated by a dashed line. **Gb.** Mean oEPSC RI in each group. The cells from chronic Δ^9-THC-treated animals showed a significantly increased RI compared to chronic vehicle-, or chronic Δ^9-THC + AM251-treated rats ($F_{3,66} = 4.54$, $p < 0.01$, 1-way ANOVA, * = $p < 0.05$, Holm-Sidak post-hoc comparison). **H.** Mean time course of the polyamine, GluR2-lacking AMPA receptor blocker NASPM on oEPSCs evoked by ChR2-activation of vHipp inputs to NAcs neurons. Mean wave forms shown above indicate peak effect of NASPM (solid line), compared to baseline (dashed line) in representative cells from chronic vehicle (gray) or chronic Δ^9-THC-treated (green) animals. NASPM caused a significant inhibition of oEPSCs only from neurons obtained from chronic Δ^9-THC-treated rats ($F_{2,20} = 4.8$, * = $p < 0.05$, 1-way ANOVA and Holm-Sidak's post-hoc test). Number of neurons/Rats: **A.** Veh: 19/8, THC: 17/7 B. Veh: 10/8, THC: 17/7 **C.** Veh:7/5, THC: 4/4 **D.** Veh: 15/7, THC: 22/7, THC+AM: 13/4 **E.** Veh: 17/5, THC: 11/4, THC+AM: 10/4 **Gb.** Veh: 17/8, THC: 24/6, THC+AM: 13/4 **H.** Veh: 6/5, THC: 10/6.

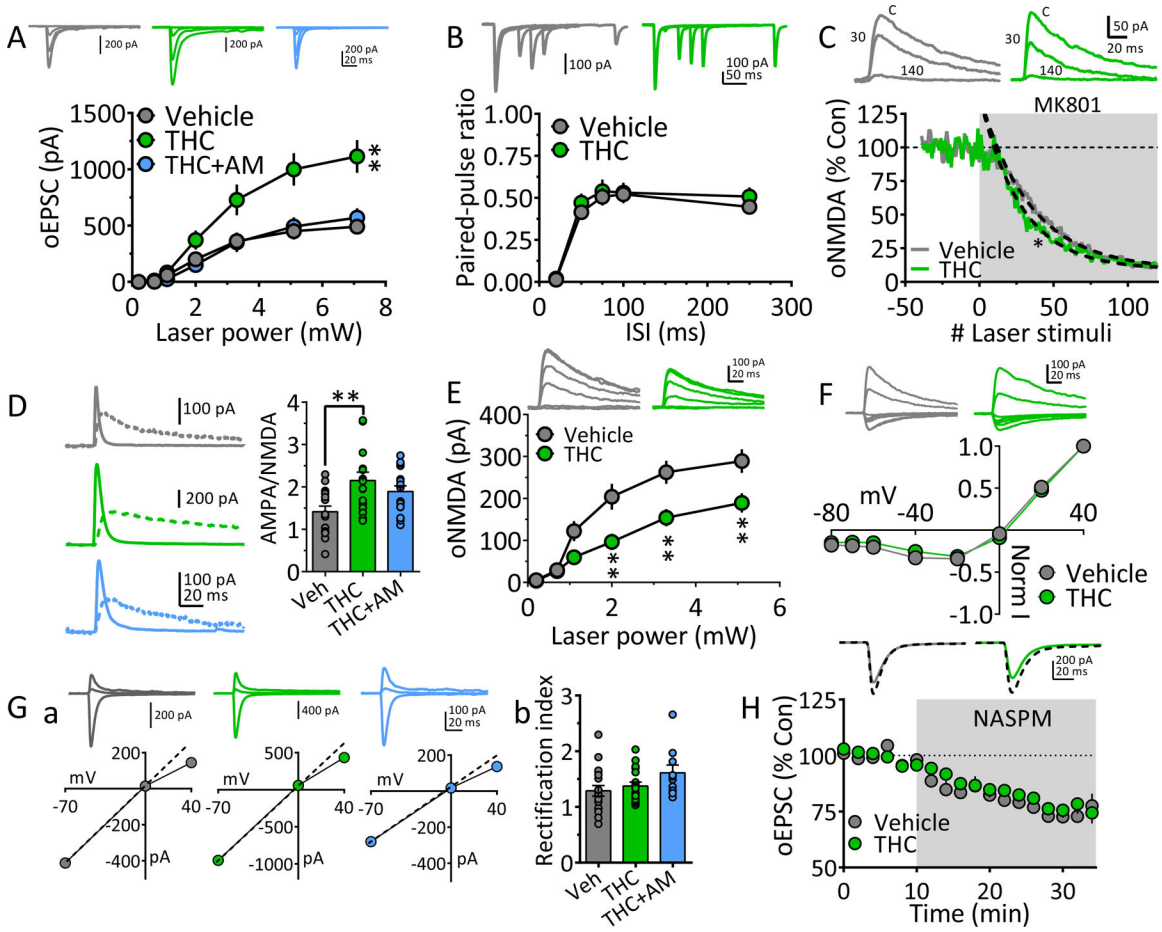

Figure 4. Mechanisms underlying strengthened BLA glutamatergic input to NAcs following chronic Δ^9-THC.

A. oEPSC I-O curves evoked by ChR2 activation of BLA axons projecting to NAcs, after chronic vehicle, Δ^9-THC, or Δ^9-THC + AM251 injections. Representative mean oEPSCs are shown at 5 laser intensities in neurons from vehicle (gray traces), Δ^9-THC (green traces), or Δ^9-THC + AM-251-injected (blue traces) rats. The strength of BLA glutamate input to NAcs neurons was significantly increased following chronic Δ^9-THC and this was prevented by AM251 (** = $F_{18,392} = 2.6$, $p < 0.001$, intensity x treatment interaction, 2-way repeated measures ANOVA). **B.** Mean PPR of BLA-evoked oEPSCs at different inter-laser pulse intervals (ISI) in NAc neurons from chronic Δ^9-THC- and vehicle injected rats. Mean representative traces from individual cells in both groups are shown above. The PPR was not significantly altered by chronic Δ^9-THC (* = $F_{12,255} = 0.3$, $p = 0.98$, ISI x treatment interaction, 2-way repeated measures ANOVA). Note that paired oEPSCs overlapped at the 20 ms ISI, thereby yielding a ratio = 0. **C.** The rate of block of ChR2-evoked oNMDA receptor oEPSCs by MK801, was significantly faster following chronic Δ^9-THC in the BLA → NAcs pathway (time-constant of oNMDA block by MK801: chronic vehicle = 34.3 stimuli, 95% confidence interval = 32.2–36.8 stimuli, n = 8 neurons, gray line; chronic Δ^9-THC = 27.9 stimuli, 95% confidence interval = 26.1–29.9 stimuli, n = 8, green line). Exponential decay time constants (**τ**) were obtained by best fit (dashed lines). Representative oNMDA waveforms from each group obtained before MK801 application (control, C), and

at 30 and 140 stimuli are shown above. **D.** AMPA/NMDA ratios show potentiated transmission at BLA → NAcs synapses. Left, representative mean waveforms of laser-evoked oEPSCs collected at −70 mV (solid line) and +40 mV (dashed line) holding potentials from chronic vehicle (gray), chronic Δ^9-THC (green), or chronic Δ^9-THC + AM251 (blue) groups. AMPA/NMDA = peak AMPA response at −70 mV divided by the peak NMDA response at +40 mV. Right, AMPA/NMDA ration group means (± s.e.m.). ** = $p < 0.01$, $F_{2,47} = 5.8$, one-way ANOVA and Holm-Sidak post-hoc comparison). **E.** I-O curves of ChR2-evoked oNMDA currents at BLA → NAcs synapses in neurons from chronic vehicle, and chronic Δ^9-THC treated rats. Representative mean oNMDA wave forms are shown above for each condition. The treatment x laser power interaction was significant ($F_{5,70} = 6.66$, $p < 0.0001$, 2-way repeated measures ANOVA; ** = $p < 0.01$, Holm-Sidak comparison), indicating a decrease in oNMDA current amplitude after chronic Δ^9-THC. **F.** Lack of chronic Δ^9-THC effect on the voltage-dependence of oNMDA currents. Representative mean traces from cells in chronic vehicle (gray), and Δ^9-THC-treated (green) groups are shown above. **G.** Δ^9-THC does not change inward rectification of ChR2-evoked AMPA receptor oEPSCs at BLA → NAcs synapses. **Ga.** Representative I-V relationships and mean AMPA oEPSCs evoked by ChR2 in the BLA → NAcs pathway at holding potentials of −70, 0, and +40 from each of the 3 groups (chronic vehicle, gray, chronic Δ^9-THC, green, and chronic Δ^9-THC + AM251, blue). A hypothetical slope = 1.0 is indicated by a dashed line. **Gb.** Mean oEPSC RI in each group. The cells from chronic Δ^9-THC-treated animals showed no significant change in RI compared to chronic vehicle-treated rats ($F_{2,44} = 2.4$, $p = 0.10$, 1-way ANOVA). **H.** Mean time course of NASPM, on oEPSCs evoked by ChR2-activation of BLA inputs to NAcs neurons. Mean wave forms shown above indicate peak effect of NASPM (solid line), compared to baseline (dashed line) in representative cells from chronic vehicle (gray) or chronic Δ^9-THC-treated (green) animals. The effect of NASPM on BLA → NAcs oEPSCs was not different between chronic vehicle and chronic Δ^9-THC groups ($F_{2,20} = 1.6$, $p = 0.23$, 1-way ANOVA and Holm-Sidak's post-hoc test). Number of cells/Rats: **A.** Veh: 23/9, THC: 16/8, THC+AM: 11/6. **B.** Veh: 20/9, THC: 16/8. **C.** Veh: 8/7, THC: 8/5. **D.** Veh: 17/8, THC: 17/7, THC+AM: 16/6. **E.** Veh: 9/7, THC: 7/5 **F.** Veh: 5/5, THC: 7/5 **Gb**. Veh: 19/8, THC: 18/7, THC+AM: 10/6 **H.** Veh: 9/6, THC: 10/7.

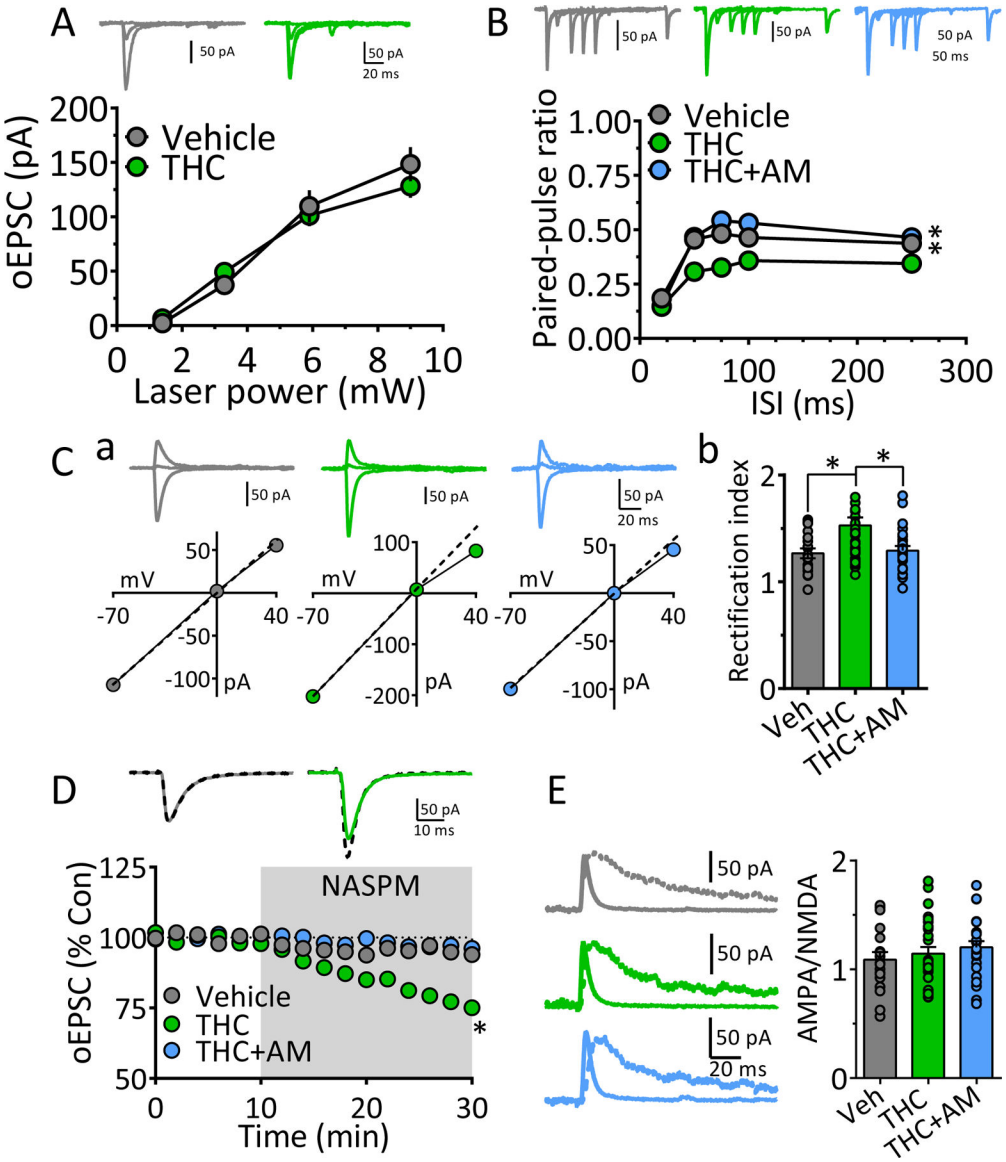

Figure 5. Homeostatic changes in VTA dopaminergic neuron glutamate input to NAcs following chronic Δ^9-THC.

A. Glutamate oEPSC I-O curves evoked by ChR2 activation of axons from THCre-positive VTA neurons projecting to NAcs, after chronic vehicle, or Δ^9-THC injections. Representative mean oEPSCs are shown at 5 laser intensities in neurons from vehicle (gray traces), or Δ^9-THC (green traces) injected THCre rats. The strength of glutamate input to NAcs neurons from the VTA was not significantly altered by chronic Δ^9-THC ($F_{3,57}$ = .9, p = 0.11, intensity x treatment interaction, 2-way repeated measures ANOVA). **B.** Mean PPR of VTA THCre neuron-evoked oEPSCs at different ISIs in NAc neurons from chronic vehicle, Δ^9-THC, and Δ^9-THC+AM251-injected rats. Mean representative traces from individual cells in both groups are shown above. The PPR was significantly reduced by chronic Δ^9-THC (** = $F_{12,328}$ = 5.3, p < 0.001, ISI x treatment interaction, 2-way repeated measures ANOVA with Holm-Sidak post-hoc test), and this was prevented by concomitant treatment with AM251 (p = 0.45, compared to vehicle). **C.** Δ^9-THC increases inward

rectification of ChR2-evoked AMPA receptor oEPSCs at VTA → NAcs synapses. **Ca.** Representative I-V relationships and mean AMPA oEPSCs evoked by ChR2 in the VTA → NAcs pathway at holding potentials of −70, 0, and +40 from each of the 3 groups (chronic vehicle, gray, Δ^9-THC, green, and Δ^9-THC + AM251, blue). A hypothetical slope = 1.0 is indicated by a dashed line. **Cb.** Mean oEPSC RI in each group. The cells from chronic Δ^9-THC-treated animals showed a significant increase in RI compared to chronic vehicle-treated rats ($F_{3,83} = 3.9$, $p < 0.01$, 1-way ANOVA; * = $p < 0.05$, Holm-Sidak post-hoc test), and this was prevented by AM251 pre-treatment ($p = 0.78$, compared to vehicle). **D.** Mean time course of the polyamine, GluR2-lacking AMPA receptor blocker, NASPM, on oEPSCs evoked by ChR2-activation of VTA glutamate inputs to NAcs neurons. Mean wave forms shown above indicate peak effect of NASPM (solid line), compared to baseline (dashed line) in representative cells from chronic vehicle (gray) or chronic Δ^9-THC-treated (green) animals. NASPM significantly reduced VTA→NAcs oEPSCs, compared to chronic vehicle, and this was prevented by AM251 ($F_{2,57} = 1.4$, $p < 0.0001$, 1-way ANOVA; * = $p < 0.001$, Holm-Sidak post-hoc test). **E.** AMPA/NMDA ratios at VTA→NAcs synapses were unaltered by Δ^9-THC ($F_{2,66} = 0.74$, $p = 0.49$; 1-way ANOVA). Left, representative mean waveforms of laser-evoked oEPSCs collected at −70 mV (solid line) and +40 mV (dashed line) holding potentials from chronic vehicle (gray), chronic Δ^9-THC (green), or chronic Δ^9-THC + AM251 (blue) groups. AMPA/NMDA = peak AMPA response at −70 mV divided by the peak NMDA response at +40 mV. Right, AMPA/NMDA ratio group means (± s.e.m.). Number of cells/Rats: **A.** Veh: 11/6, THC: 10/6. **B.** Veh: 25/10, THC: 15/12, THC+AM: 30/8. **Cb.** Veh: 18/10, THC: 31/12, THC+AM: 24/8. **D.** Veh: 13/10, THC: 30/12, THC+AM: 8/7. **E.** Veh: 18/10, THC: 27/12, THC+AM: 24/8.

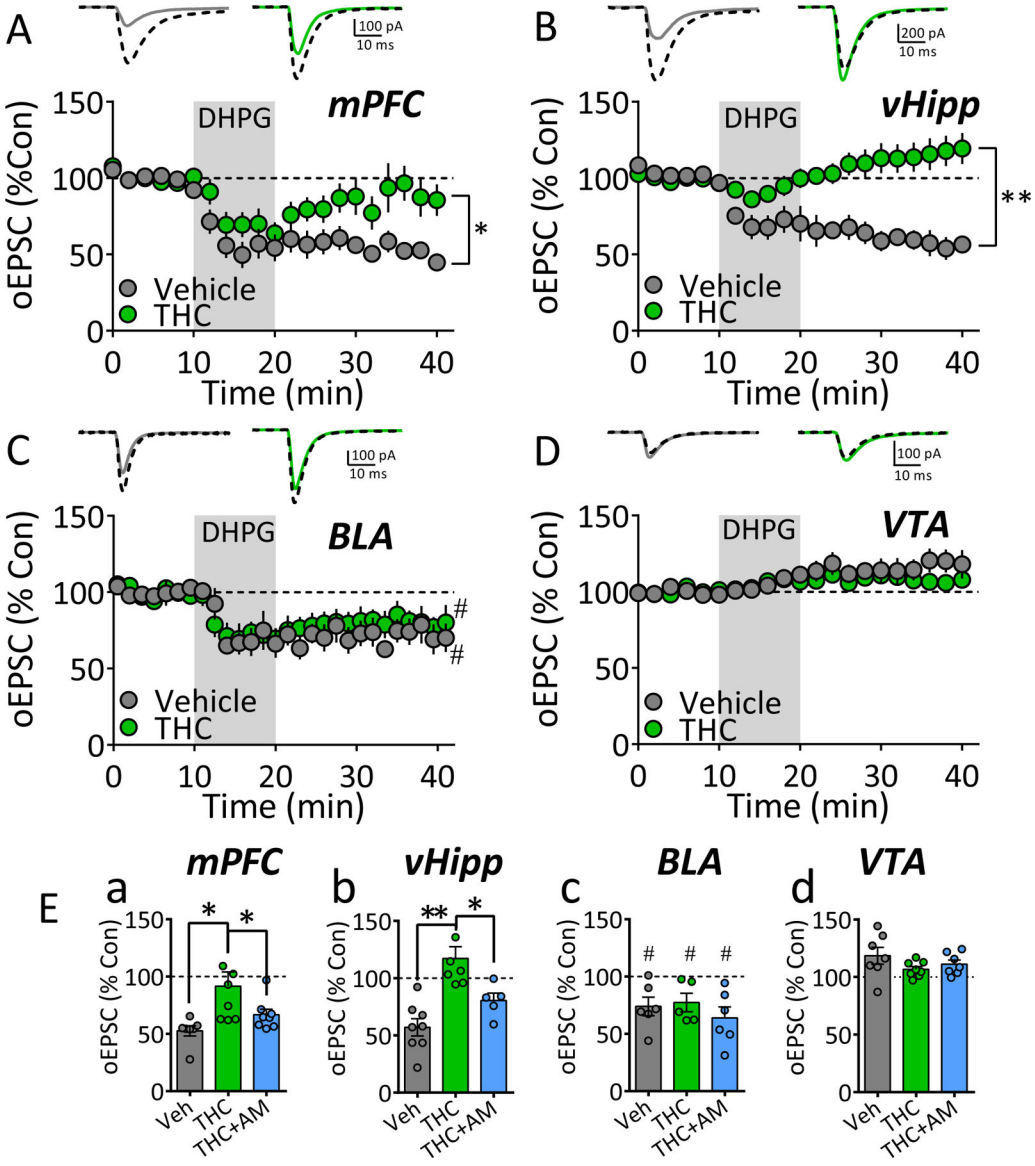

Figure 6. Chronic Δ^9-THC differentially alters mGluRI-induced synaptic plasticity distinct NAcs glutamate afferents.

A-D. Effects of a 10 min application of the mGluRI agonist, DHPG, on oEPSCs evoked via ChR2-activation of glutamate afferents to the NAcs. Shown for each brain region is a mean time-course of the oEPSCs, normalized to 100 % of control, for the chronic Δ^9-THC and vehicle groups (below) and representative averaged waveforms from individual cells from each group (above). In each instance, control mean oEPSCs collected before DHPG application are indicated by black dashed lines, whereas oEPSCs averaged from individual sweeps, collected from minute 35 to minute 42, are indicated by solid lines in neurons from vehicle- (gray) or Δ^9-THC-treated (green) animals. **A.** Effects of DHPG on mPFC afferents to NAcs (* = $p < 0.001$, repeated measures ANOVA, $F_{20,260} = 2.7$, time vs. treatment interaction). **B.** Effects of DHPG on oEPSCs evoked by ChR2-activation of vHipp glutamate afferents to the NAcs (** = $p < 0.0001$, repeated measures ANOVA, $F_{20,260} = 13.2$, time vs. treatment interaction). **C.** Effects of DHPG on oEPSCs evoked by ChR2-activation of BLA

glutamate afferents to the NAcs shows that DHPG-LTD was significant compared to baseline in all groups (one-way ANOVA, $F_{3,20} = 5.1$, $p = 0.009$; # = $p < 0.05$, Newman-Keuls post-hoc test), but there was no difference in LTD among groups. **D.** Effects of DHPG on oEPSCs evoked by ChR2-activation of VTA THCre neuron glutamate afferents to the NAcs (time vs. treatment interaction not significant, repeated measures ANOVA, $F_{20,260} = 1.4$,). **E.** Summary of DHPG effect on normalized oEPSCs, evoked by ChR2-activation of afferents arising from mPFC **(a)**, vHipp **(b)**, BLA **(c)**, and the VTA **(d)** for the chronic vehicle (Veh), chronic Δ^9-THC, and chronic Δ^9-THC + AM251 (THC+AM) groups. * = $p < 0.05$, ** = $p < 0.0001$, 1-way ANOVA with Holm-Sidak post-hoc comparison. # = $p < 0.05$, 1-way ANOVA with Newman-Keuls post-hoc. Number of neurons/Rat per group: **A.** Veh: 7/6, THC: 8/5. **B.** Veh: 8/5, THC: 7/5. **C.** Veh: 5/5, THC: 6/5. **D.** Veh: 7/6, THC: 9/6. **Ea.** Veh: 7/6, THC: 8/5, THC+AM: 8/5. **Eb.** Veh: 8/5, THC: 7/5, THC+AM: 5/4. **Ec.** Veh: 6/5, THC: 5/5, THC+AM: 6/5. **Ed.** Veh: 7/6, THC: 8/6, THC+AM: 7/5.

KEY RESOURCES TABLE

Resource Type	Specific Reagent or Resource	Source or Reference	Identifiers	Additional Information
Add additional rows as needed for each resource type	Include species and sex when applicable.	Include name of manufacturer, company, repository, individual, or research lab. Include PMID or DOI for references; use “this paper” if new.	Include catalog numbers, stock numbers, database IDs or accession numbers, and/or RRIDs. RRIDs are highly encouraged; search for RRIDs at https://scicrunch.org/resources.	Include any additional information or notes if necessary.
Bacterial or Viral Strain	AAV5/CamKII-hChR2(H134R)-EYFP-WPRE-PA	University of North Carolina Vector Core	N/A	
Bacterial or Viral Strain	AAV5/Ef1a-DIO-hChR2(H134R)-EYFP	University of North Carolina Vector Core	N/A	
Chemical Compound or Drug	(-)-trans-Δ9-Tetrahydrocannabinol	NIDA Drug Supply	RTI Log Number: 14308–0918-53	
Chemical Compound or Drug	DL-AP5	Tocris	Cat. No. 0105	
Chemical Compound or Drug	DNQX disodium salt	Tocris	Cat. No. 2312	
Chemical Compound or Drug	Naspm trihydrochloride	Tocris	Cat. No. 2766	
Chemical Compound or Drug	(S)-3,5-DHPG	Tocris	Cat. No. 0805	
Chemical Compound or Drug	AM251	Tocris	Cat. No. 1117	
Chemical Compound or Drug	picrotoxin	Sigma-Aldrich	P1675	
Chemical Compound or Drug	(+)-MK-801 hydrogen maleate	Sigma-Aldrich	M107	
Chemical Compound or Drug	Ifenprodil (+)-tartrate salt	Sigma-Aldrich	I2892	
Organism/Strain	Rat: Long-Evans, male	Charles Rivers	Strain Code:006	
Organism/Strain	Rat: TH-cre	NIDA Transgenic facility	None	
Software; Algorithm	WinLTP	WinLTP Ltd. and The University of Bristol,	RRID:SCR_008590	
Software; Algorithm	Clampfit(v9.0)	Molecular Devices		
Software; Algorithm	GraphPad Prism 6.0	GraphPad Software		
Other				